Cerebral Cortex, June 2021;31: 3047–3063

doi: 10.1093/cercor/bhaa411
Advance Access Publication Date: 16 February 2021
Original Article

ORIGINAL ARTICLE

Decoding Neural Representations of Affective Scenes in Retinotopic Visual Cortex

Ke Bo[1], Siyang Yin[1], Yuelu Liu[2], Zhenhong Hu[1], Sreenivasan Meyyappan[1], Sungkean Kim[1], Andreas Keil[3] and Mingzhou Ding[1]

[1]J. Crayton Pruitt Family Department of Biomedical Engineering, University of Florida, Gainesville, FL 32611, USA, [2]Center for Mind and Brain, University of California, Davis, CA 95618, USA and [3]Department of Psychology, University of Florida, Gainesville, FL 32611, USA

Address correspondence to Mingzhou Ding. Email: mding@bme.ufl.edu; Andreas Keil. Email: akeil@ufl.edu.

Abstract

The perception of opportunities and threats in complex visual scenes represents one of the main functions of the human visual system. The underlying neurophysiology is often studied by having observers view pictures varying in affective content. It has been shown that viewing emotionally engaging, compared with neutral, pictures (1) heightens blood flow in limbic, frontoparietal, and anterior visual structures and (2) enhances the late positive event-related potential (LPP). The role of retinotopic visual cortex in this process has, however, been contentious, with competing theories predicting the presence versus absence of emotion-specific signals in retinotopic visual areas. Recording simultaneous electroencephalography–functional magnetic resonance imaging while observers viewed pleasant, unpleasant, and neutral affective pictures, and applying multivariate pattern analysis, we found that (1) unpleasant versus neutral and pleasant versus neutral decoding accuracy were well above chance level in retinotopic visual areas, (2) decoding accuracy in ventral visual cortex (VVC), but not in early or dorsal visual cortex, was correlated with LPP, and (3) effective connectivity from amygdala to VVC predicted unpleasant versus neutral decoding accuracy, whereas effective connectivity from ventral frontal cortex to VVC predicted pleasant versus neutral decoding accuracy. These results suggest that affective scenes evoke valence-specific neural representations in retinotopic visual cortex and that these representations are influenced by reentry signals from anterior brain regions.

Key words: affective scenes, amygdala, late positive potential, multivariate pattern analysis, visual cortex

Introduction

Visual media are a major source of information as well as entertainment and, as such, have become a central element in people's lives. Using pictures or videos of varying emotional content to elicit strong viewer response is a key aspect of visual media usage. Studies have shown that compared with affectively neutral visual stimuli, emotionally engaging visual stimuli are viewed longer (Bradley et al. 2001), rated as being more arousing (Lang et al. 1993), and accompanied by heightened autonomic as well as neurophysiological responses (Bradley 2009). Because of these properties, viewing affective pictures has been extensively used as a laboratory model of emotional engagement, resulting in an immense literature (Bradley et al. 2012), which includes studies aiming to characterize the neurophysiological basis of emotional picture perception (Sabatinelli et al. 2011; Frank and Sabatinelli 2017).

Functional magnetic resonance imaging (fMRI) studies have shown that viewing emotionally arousing pictures, relative to neutral pictures, prompts higher blood oxygen level-dependent (BOLD) activity in a widespread network of regions, including the amygdaloid complex, pulvinar, medial prefrontal cortex (MPFC), orbitofrontal cortex, and widespread extrastriate parieto-occipital and temporal cortices, with strong responses in higher-order, but not retinotopic, visual areas (Lang et al. 1998;

Bradley et al. 2003, 2015; Norris et al. 2004; Sabatinelli et al. 2005). Over the past decade, however, evidence from other measurement modalities [e.g., electroencephalography (EEG) and event-related potential (ERP); Thigpen et al. 2017], ranging from experimental animals (Li et al. 2019) to computational modeling (Kragel et al. 2019), has supported the strong involvement of early, retinotopic visual areas in representing emotional content. Although these findings are in line with behavioral studies showing that emotion facilitates early visual processing (Phelps et al. 2006), hemodynamic imaging work has to date failed to observe consistent differential activation between emotional and neutral pictures in primary visual cortex and other retinotopic areas (Lang et al. 1998; Sabatinelli et al. 2014).

The lack of consistent findings may be partly attributable to the limitations of univariate analysis methods used in most of the prior fMRI studies. The recent advent of multivariate pattern analysis (MVPA) provides a potential avenue to close the gap. MVPA examines voxel-level activation within a region of interest (ROI) as a multivariate pattern and yields a decoding accuracy to quantify the difference between patterns of different classes of stimuli at the single subject level (Norman et al. 2006). This technique has been successfully applied in affective neuroscience and has extended the field beyond univariate studies by decoding multivoxel neural representations of emotion within specific brain regions (Ethofer et al. 2009; Peelen et al. 2010) and within large-scale neural networks (Baucom et al. 2012; Saarimäki et al. 2015; Bush et al. 2017). Building on this body of work, the present study applied MVPA to systematically define the multivoxel patterns evoked by emotional stimuli within specific regions along the retinotopic visual hierarchy, extending from primary visual cortex (V1) to intraparietal cortex along the dorsal pathway and to parahippocampal cortex (PHC) along the ventral pathway, and tested the hypothesis that voxel patterns in retinotopic cortex code for valence-specific emotional content.

If visuocortical activation patterns encode emotional content, this would raise the question regarding the origin of these patterns. Two competing but not mutually exclusive groups of hypotheses have been advanced to account for emotion-specific modulations of activity in retinotopic visual areas. First, the so-called reentry hypothesis states that the increased visual activation evoked by affective pictures results from reentrant feedback, meaning that signals arising in subcortical emotion-processing structures such as the amygdala propagate to visual cortex to facilitate the processing of motivationally salient stimuli (Sabatinelli et al. 2005; Lang and Bradley 2010; Pessoa 2010). According to tracer studies in macaques, such reentrant projections exist, and they are more sparse for retinotopic, compared with anterior visual regions (Amaral et al. 2003; Freese and Amaral 2005), consistent with findings from univariate fMRI studies (Sabatinelli et al. 2011) and from ERP studies (Keil et al. 2002). Neuroimaging studies have also lent support to the reentry hypothesis by comparing enhanced hemodynamic responses evoked by emotionally arousing stimuli in the amygdala and in the visual cortex (Lane et al. 1997; Pessoa et al. 2002; Sato et al. 2004; Sabatinelli et al. 2005). For example, a fast-sample fMRI study demonstrated that the response enhancement in the amygdala precedes that in extrastriate visual cortex (Sabatinelli et al. 2009). Moreover, amygdala and visual cortical activity strongly covary during emotional picture viewing (Sabatinelli et al. 2005; Kang et al. 2016). Critically, patients with amygdala lesions showed no enhancement in visual cortical activity when fearful faces were presented even though their visual system remains intact (Vuilleumier et al. 2004). This evidence suggests that amygdala is possibly a source of the reentrant signals.

A second group of hypotheses states that sensory cortex, including retinotopic visual areas, may itself code for emotional qualities of a stimulus, without the necessity for recurrent processing (see Miskovic and Anderson 2018 for a review). Evidence supporting this hypothesis comes from empirical studies in experimental animals (Weinberger 2004; Li et al. 2019) as well as in human observers (Thigpen et al. 2017), in which the extensive pairing of simple sensory cues such as tilted lines or sinusoidal gratings with emotionally relevant outcomes shapes early sensory responses (Miskovic and Keil 2012). Beyond simple cues, recent computational work using deep neural networks has also suggested that visual cortex may intrinsically represent emotional value as contained in complex visual media such as video clips of varying affective content (Kragel et al. 2019).

The competing notions discussed above may be aligned under the perspective that novel, complex emotional scenes initially elicit widespread recurrent processing, including between retinotopic visual and limbic/frontal areas, prompting emotion-specific signaling in visual cortex (Bradley et al. 2012). If repeated extensively, critical stimulus properties of emotional stimuli may well be represented natively in retinotopic visual areas (McTeague et al. 2015). Hampering advancement of either group of hypotheses, however, is the fact that it is unclear to what extent retinotopic visual areas contain information specific to emotional content and—if so—how this information emerges. Here, we use multimodal neuroimaging together with novel computational techniques to examine the hypotheses that (1) retinotopic visual cortex contains voxel pattern information that is specific to emotional content and (2) these patterns are formed under the influence of reentrant signals from anterior brain structures, for example, the amygdala.

Recurrent processing such as the engagement of large-scale reentrant feedback projections may be assessed in different ways. First, slow hemodynamic interarea interactions can be quantified through suitable BOLD-based functional connectivity analyses, allowing us to quantify, for example, the functional interaction between amygdala and visual cortex (Freese and Amaral 2005; Sabatinelli et al. 2009, 2014). Second, recurrent processing may be characterized by leveraging the greater time resolution of scalp-recorded brain electric activity. For example, human EEG studies have shown that the late positive potential (LPP), a positive-going, long-lasting ERP component that starts about 300–400 ms after picture onset, may serve as an index of signal reentry. Robust LPP enhancement has been found when comparing emotion stimuli with neutral stimuli (Cacioppo et al. 1994; Schupp et al. 2000; Keil et al. 2002; Pastor et al. 2008). Moreover, the amplitude of the LPP enhancement is linearly related to BOLD activity, both in visual cortex and in the amygdala (Sabatinelli et al. 2009, 2013; Liu et al. 2012), and is thought to reflect heightened processing of motivational relevant stimuli in perceptual, memory, and motor systems, associated with signal reentry (Vuilleumier 2005; Hajcak et al. 2006; Lang and Bradley 2010).

We recorded simultaneous EEG-fMRI data from subjects viewing pleasant, unpleasant, and neutral pictures selected from the International Affective Picture System (IAPS; Lang et al. 1997). Given the questions and hypotheses stated above, the primary focus here was on the fMRI data, with the EEG data used mainly to yield the LPP amplitude for each participant, serving as a proxy for recurrent processing among visual and extravisual regions in the brain's emotion network (Liu et al. 2012).

In addition to conventional univariate BOLD activation and LPP analyses, BOLD responses were estimated on a trial-by-trial basis, and MVPA was applied to decode single-trial BOLD responses to investigate if the neural patterns within retinotopic visual cortex were distinct between emotional and neutral scenes. Strength of reentrant feedback indexed by LPP amplitude and frontotemporal→visual cortex effective connectivity (EC) was correlated with MVPA decoding accuracy in visual cortex to test the impact of signal reentry on neural representations of emotional stimuli.

Materials and Methods

Overview

Simultaneous EEG-fMRI was recorded from human subjects viewing pleasant, unpleasant, and neutral pictures from the IAPS library (Lang et al. 1997). Following signal preprocessing, univariate and multivariate analyses were applied to examine the neural representations of affective pictures in retinotopic visual cortex. To help with reading, a table explaining the abbreviated labels of each investigated brain region is included in the supplementary materials (Supplementary Table S1).

Participants

The experimental protocol was approved by the Institutional Review Board of the University of Florida. A total of 26 healthy volunteers with normal or corrected-to-normal vision gave written informed consent and participated in this study. Before the magnetic resonance imaging (MRI) scan, two subjects withdrew from the experiment. In addition, data from four participants were discarded due to artifacts generated by excessive movements inside the scanner. The data from the remaining 20 subjects were analyzed and reported here (10 women; mean age: 20.4 ± 3.1).

Stimuli

The stimuli consisted of 60 gray-scaled pictures selected from the IAPS (Lang et al. 1997). Their IAPS IDs are as follows: (1) 20 pleasant pictures: 4311, 4599, 4610, 4624, 4626, 4641, 4658, 4680, 4694, 4695, 2057, 2332, 2345, 8186, 8250, 2655, 4597, 4668, 4693, 8030; (2) 20 neutral pictures: 2398, 2032, 2036, 2037, 2102, 2191, 2305, 2374, 2377, 2411, 2499, 2635, 2347, 5600, 5700, 5781, 5814, 5900, 8034, 2387; (3) 20 unpleasant pictures: 1114, 1120, 1205, 1220, 1271, 1300, 1302, 1931, 3030, 3051, 3150, 6230, 6550, 9008, 9181, 9253, 9420, 9571, 3000, 3069. The pleasant pictures included sports scenes, romance, and erotic couples and had an average valence rating of 7.0 ± 0.45. The unpleasant pictures included threat/attack scenes and bodily mutilations and had an average valence rating of 2.8 ± 0.88. The neutral pictures consisted of images containing landscapes and neutral humans and had an average valence rating of 6.3 ± 0.99. The arousal ratings of these pictures are as follows: pleasant (5.8 ± 0.90), unpleasant (6.2 ± 0.79), both being higher than that of neutral pictures (4.2 ± 0.97) (all ratings are based on a 1–9 scale). To minimize confounds, across categories, pictures were chosen to be similar overall in composition and in rated complexity and matched in picture file size. In addition, no significant difference was found across categories in entropy ($F = 1.05$, $P = 0.35$) and in pixel contrast ($F = 0.52$, $P = 0.60$).

Procedure

As shown in Figure 1, each IAPS picture was displayed on a magnetic resonance (MR)-compatible monitor for 3 s, which was followed by a variable (2800 or 4300 ms) interstimulus interval. There were five sessions. Each session comprised 60 trials corresponding to the 60 different pictures. The same 60 pictures were shown in each session, but the order of picture presentation was randomized from session to session. Stimuli were presented on the monitor placed outside the scanner and viewed via a reflective mirror. Participants were instructed to maintain fixation on the cross at the center of the screen during the whole session. After the experiment, participants were instructed to rate the hedonic valence and emotional arousal level of 12 representative IAPS pictures (four pleasant, four neutral, and four unpleasant), which were not part of the 60-picture set. The rating was done using a paper and pencil version of the self-assessment manikin (Bradley and Lang 1994). As shown in Supplementary Table S2 of the supplementary materials, the ratings of the 12 pictures by the participants are consistent with the normative ratings of these pictures (Lang et al. 1997).

Data Acquisition

Functional MRI data were collected on a 3 T Philips Achieva scanner (Philips Medical Systems), with the following parameters: echo time, 30 ms; repetition time, 1.98 s; flip angle, 80°; slice number, 36; field of view, 224 mm; voxel size, $3.5 \times 3.5 \times 3.5$ mm; matrix size, 64×64. Slices were acquired in ascending order and oriented parallel to the plane connecting the anterior and posterior commissure. T_1-weighted high-resolution structural image was also obtained.

EEG data were recorded simultaneously with fMRI using a 32-channel MR-compatible EEG system (Brain Products GmbH). A total of 31 sintered Ag/AgCl electrodes were placed on the scalp according to the 10–20 system, and one additional electrode was placed on subject's upper back to monitor electrocardiograms (ECGs). The recorded ECG was used to detect heartbeat events and assist in the removal of the cardioballistic artifacts. The EEG channels were referenced to the FCz electrode during recording. EEG signal was recorded with an online 0.1–250 Hz band-pass filter and digitized to 16-bit at a sampling rate of 5 kHz. The EEG recording system was synchronized with the scanner's internal clock throughout recording to ensure the successful removal of the gradient artifact in subsequent preprocessing.

Data Preprocessing

The fMRI data were preprocessed with SPM (http://www.fil.ion.ucl.ac.uk/spm/). The first five volumes from each session were discarded to eliminate artifacts caused by the transient instability of scanner. Slice timing was corrected using interpolation to account for differences in slice acquisition time. The images were then corrected for head movement by spatially realigning them to the sixth image of each session, normalized and registered to the Montreal Neurological Institute template, and resampled to a spatial resolution of $3 \times 3 \times 3$ mm. The transformed images were smoothed by a Gaussian filter with a full width at half maximum of 8 mm. Low-frequency temporal drift was removed from the functional images by applying a high-pass filter with a cutoff frequency of 1/128 Hz.

The EEG data were first processed using Brain Vision Analyzer 2.0 (Brain Products GmbH) to remove scanner artifacts. For

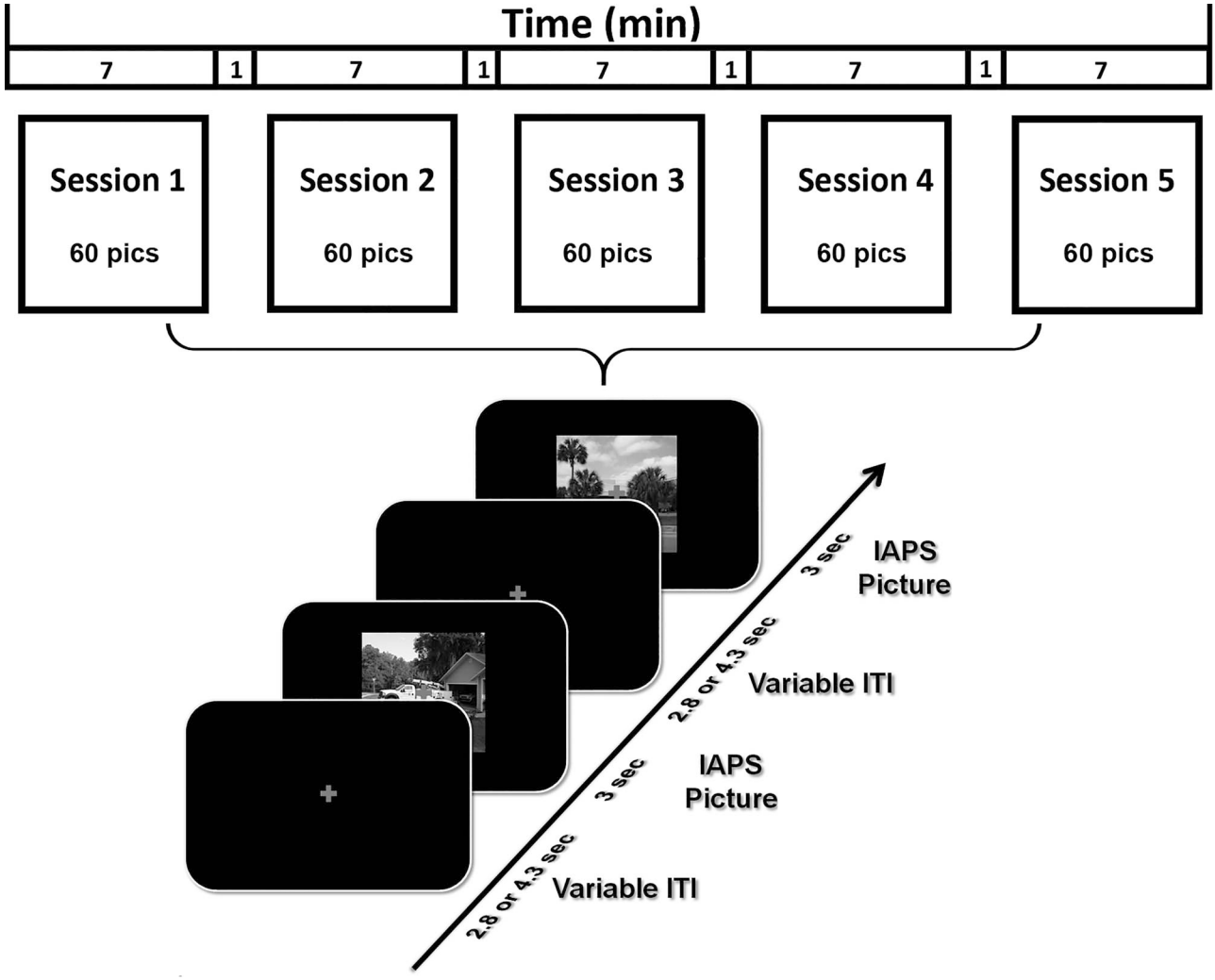

Figure 1. Picture viewing paradigm. There were five sessions. Each session lasted 7 min. A total of 60 IAPS pictures, including 20 pleasant, 20 unpleasant, and 20 neutral, were presented in each session, the order of which randomly varied from session to session. Each picture lasted 3 s and was followed by a fixation period referred to as intertrial interval (ITI) (2.8 or 4.3 s). Participants were required to fixate on the cross in the center of screen throughout the session.

removing gradient artifacts, a modified version of the original algorithm proposed for this purpose was applied (Allen et al. 2000). Briefly, an artifact template was created by segmenting and averaging the data according to the onset of each volume and subtracted from the raw EEG data. The cardioballistic artifact was removed by an average artifact subtraction method (Allen et al. 1998). Specifically, R peaks were detected in the low-pass-filtered ECG signal and used to establish a delayed average artifact template over 21 consecutive heartbeat events by sliding-window approach. The artifact was then subtracted from the original EEG signal. After gradient and cardioballistic artifacts were removed, the EEG data were low-pass filtered with the cutoff set at 50 Hz, downsampled to 250 Hz, re-referenced to the average reference, and exported to EEGLAB for further processing (Delorme and Makeig 2004). Second-order blind identification (Belouchrani et al. 1993) was then applied to correct for eye blinking, residual cardioballistic, and movement-related artifacts. The artifact-corrected data were epoched from −300–2000 ms with 0 ms denoting picture display onset. The prestimulus baseline was defined as −300–0 ms for ERP analysis.

Single-Trial Estimation of fMRI-BOLD

Trial-by-trial picture-evoked BOLD signal was estimated by using the beta series method (Mumford et al. 2012). In this method, the trial of interest was represented by one regressor and all the other trials were represented by another regressor. Six motion regressors were also included to account for any movement-related artifacts during scan. Repeating the process for all the trials, we obtained the BOLD response to each picture presentation in each brain voxel. These single-trial BOLD responses were used in the MVPA decoding analysis.

ROIs in Retinotopic Visual Cortex

ROIs were defined according to a recently published probabilistic visual retinotopic atlas (Wang et al. 2015). A total of 17 ROIs in the retinotopic visual atlas were included: V1v, V1d, V2v, V2d, V3v, V3d, V3a, V3b, hV4, ventral occipital (VO1), VO2, PHC1, PHC2, lateral occipital (LO1), LO2, human middle temporal (hMT), and intraparietal sulcus (IPS) (Fig. 3A). The homologous regions from the two hemispheres were combined, and the IPS ROI was

formed by combining the voxels from IPS0, IPS1, IPS2, IPS3, IPS4, and IPS5. There were a total of 17 ROIs.

MVPA

MVPA was performed by the linear support vector machine (SVM) method using the LibSVM package (http://www.csie.ntu.edu.tw/~cjlin/libsvm/) (Chang and Lin 2011). Single-trial voxel patterns evoked by pleasant, unpleasant, and neutral pictures were decoded in a pairwise fashion (e.g., pleasant vs. neutral) within 17 retinotopic ROIs. The classification accuracy was calculated by 10-fold validation. Specifically, all the data was divided into 10 equal subdatasets, nine of which comprised training data to train the classifier and the remaining one of which was used for testing. The decoding accuracies of 10 such procedures were averaged. To further ensure the stability of the decoding result, we repeated 10-fold partition 100 times, conducted the same procedure to acquire decoding accuracies for each partition, and averaged the accuracies to yield the decoding accuracy for each ROI. Repeating the process for each participant, group-level decoding accuracy was computed by averaging individual accuracies across 20 participants. A nonparametric permutation-based technique (Stelzer et al. 2013) was applied to test whether the statistical significance of decoding accuracy was above chance level for each ROI. At the individual subject level, the class labels were randomly shuffled 100 times, and each shuffled run generated one chance-level decoding accuracy. At the group level, one of the chance-level decoding accuracies was extracted randomly from each subject and averaged across subjects. This process was repeated 10^5 times to obtain an empirical distribution of the chance-level accuracy at the group level for each ROI. The accuracy corresponding to $P = 0.001$ in the probability distribution of the permutation test was used as the threshold to determine whether decoding accuracy is above chance level.

EC Via Directed Acyclic Graphs

Functional connectivity analysis is typically based on cross-correlation analyses. Cross-correlation has a key limitation: It does not provide directional information. To test the potential sources of reentrant signals, we thus used an EC measurement called the directed acyclic graph (DAG), derived from linear non-Gaussian acyclic models (LiNGAM) (Shimizu et al. 2006, 2011). LiNGAM is a linear non-Gaussian variant of structural equation modeling. It has been successfully applied in fMRI work to assess EC (Schlösser et al. 2003; Marrelec et al. 2009; Liu et al. 2015). Briefly, LiNGAM estimates causal order using the recurrent regression method to find exogenous variables in the system and analyze the connection strength via least squares regression. The algorithm achieves better efficiency when prior knowledge is provided. In the current work, given the evidence from prior anatomical and causality studies showing direct synaptic connection and significantly greater directional connection from amygdala to the ventral visual system (Amaral et al. 2003; Sabatinelli et al. 2014), we provided the prior knowledge that signal in amygdala leads the directional connection towards ventral visual cortex (VVC) to the algorithm. With such prior knowledge, the estimation of LiNGAM is equivalent to a structural equation model. The connection coefficient from LiNGAM is used to represent EC strength.

Two types of EC analysis were considered: one based on a priori considerations and the other a seed-based whole-brain analysis. In the analysis based on the a priori considerations, ROIs were the amygdala and the VVC. Amygdala ROI consisted of two spherical masks of 5 mm in radius centered at [−16, 0, −24] and [20, 0, −20] (Hamann et al. 2004). The VVC ROI consisted of retinotopic visual regions VO1, VO2, PHC1, and PHC2. For the seed-based whole-brain analysis, VVC was used as the seed, and the EC into VVC was assessed for all the voxels in the brain.

ERP Analysis

The LPP was used here as an index of recurrent processing among brain regions in the emotion network (Liu et al. 2012). Preprocessed EEG data (see Data Preprocessing) was low-pass filtered at 30 Hz and averaged within each picture category to yield the ERP for that category. Figure 2C showed grand average LPPs at Pz for the three categories of pictures (left) and the topographic maps of LPP differences between affective scenes and neutral scenes (right). Here, the choice of using Pz as the site for estimating LPP was based on two considerations: (1) best separation between emotional and neutral categories and (2) balance between pleasant and unpleasant images. A paired t-test comparing the two topographic maps in Figure 2C (right) demonstrated that Pz met these two conditions. In addition to grand average LPP, for each subject, the LPP amplitude was obtained by using the time interval of 500 ms in duration around the peak of LPP (Liu et al. 2012).

Results

Univariate Analysis of fMRI BOLD

Relative to neutral pictures, unpleasant pictures activated bilateral occipitotemporal junctions, pre/postcentral gyrus, bilateral ventral lateral prefrontal cortices, left orbital frontal cortex, bilateral amygdalae/hippocampi, and insula (Fig. 2A). Other activated areas included bilateral posterior parietal cortices, fusiform gyrus, lingual gyrus, and temporal pole. Pleasant pictures, relative to neutral pictures, activated bilateral occipitotemporal junctions, bilateral posterior parietal cortices, right amygdala/hippocampus, bilateral inferior frontal gyrus (IFG), MPFC, and left orbital frontal cortex (Fig. 2B). Other activated areas included fusiform gyrus, lingual gyrus, middle frontal gyrus, and temporal pole. Thus, in addition to limbic and frontal emotion-processing structures, both pleasant and unpleasant affective scenes, relative to neutral scenes, more strongly engaged regions of the higher-order visual cortex, consistent with previous reports (Lane et al. 1997; Phan et al. 2002; Liu et al. 2012; see the review by Sabatinelli et al. 2011). Statistically, the activation map in Figure 2 was thresholded at $P < 0.05$, corrected for multiple comparisons by the false discovery rate (FDR) method. The transformed effect size of activation threshold is $d = 0.62$ ($t = 2.78$) for unpleasant versus neutral and $d = 0.63$ ($t = 2.82$) for pleasant versus neutral.

ERP Analysis

Grand average ERPs at Pz are shown for each of the three categories of pictures in Figure 2C. The LPP, starting ~300 ms after picture onset, was higher for pleasant and unpleasant pictures compared with neutral pictures. A one-way analysis of variance confirmed that LPP amplitude was significantly different among the three conditions ($F = 21.96$, $P < 0.05$, $\eta^2_{\text{partial}} = 0.53$). Post hoc analysis confirmed that the mean LPP amplitudes for both

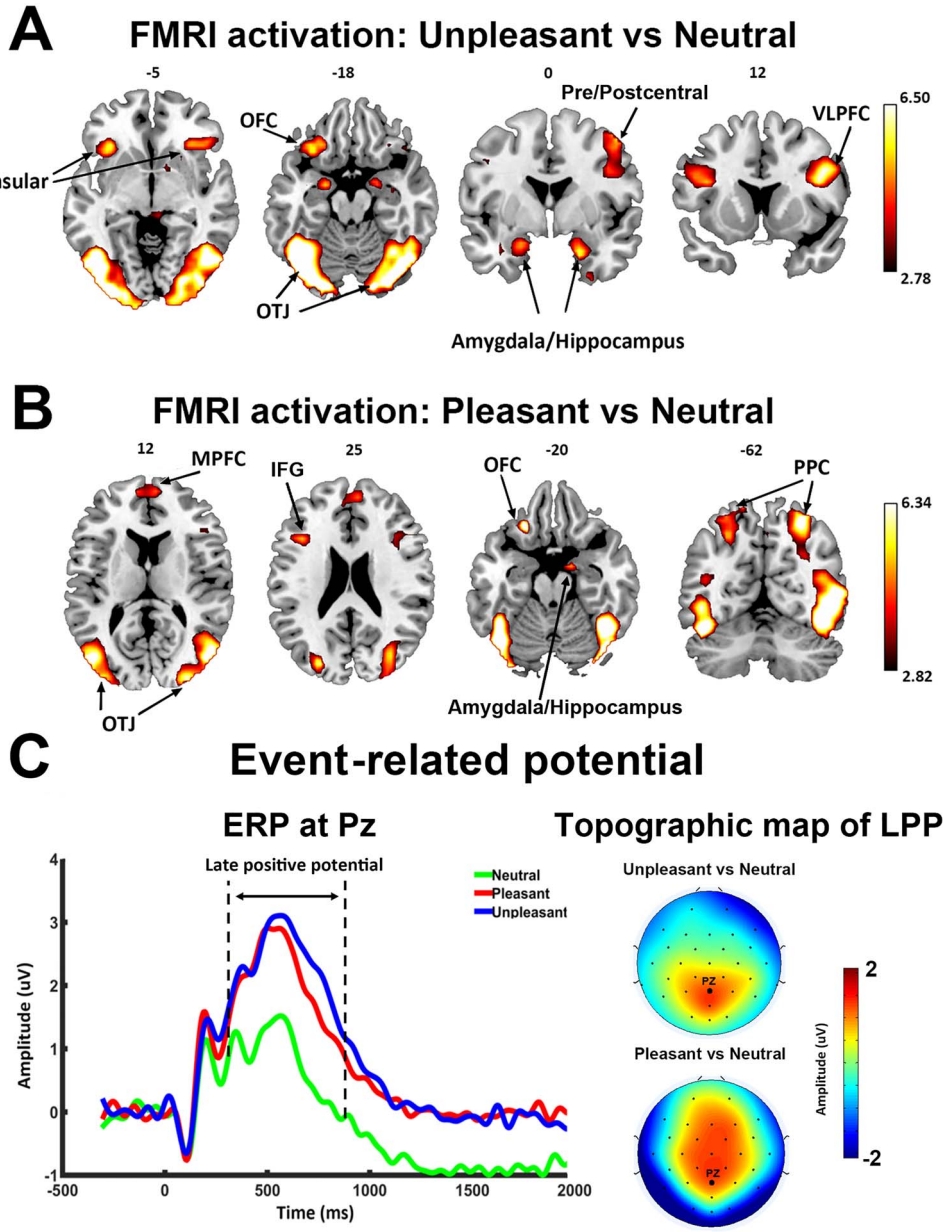

Figure 2. Univariate fMRI and ERP analysis. (*A*) Activation map ($P < 0.05$, FDR) contrasting unpleasant versus neutral pictures. (*B*) Activation map ($P < 0.05$, FDR) contrasting pleasant versus neutral pictures. (*C*) Grand average ERP ($n = 20$) at Pz showing ERP evoked by three classes of pictures (left) and scalp topography of LPP enhancement (300–800 ms after picture onset). PPC, posterior parietal cortex; OFC, orbital frontal cortex; OTJ, occipitotemporal junction.

pleasant (1.972 ± 1.882 μV) and unpleasant (2.263 ± 2.052 μV) pictures were significantly larger than that for neutral pictures (0.781 ± 1.860 μV; pleasant vs. neutral: $t(19) = 4.41$, $P < 0.001$, $d = 0.99$; unpleasant vs. neutral: $t(19) = 6.52$, $P < 0.001$, $d = 1.46$); no significant difference was found in LPP amplitude between the pleasant and unpleasant categories ($t(19) = 1.39$, $P = 0.18$, $d = 0.31$). The topographical maps depicting the scalp distribution of differential LPP amplitudes are also shown in Figure 2C. This distribution showed that LPP enhancement in pleasant versus neutral and in unpleasant versus neutral was both characterized by a centroparietal/centrofrontal distribution of positive voltage. These findings are consistent with numerous previous reports using the same paradigm (Cuthbert et al. 2000; Keil et al. 2001; Schupp et al. 2003; Liu et al. 2012).

MVPA Analysis of fMRI BOLD

For MVPA, 17 retinotopic ROIs were selected according to a recently published probabilistic atlas (Wang et al. 2015), including V1d, V1v, V2d, V2v, V3v, V3d, hV4, VO1, VO2, PHC1, PHC2, hMT, LO1, LO2, V3a, V3b, and IPS (Fig. 3A). The accuracy of decoding between unpleasant and neutral and between pleasant and neutral was shown for each ROI in Figure 3B. Across all visual ROIs, both unpleasant versus neutral decoding as well as pleasant versus neutral decoding accuracy was well above

chance level, as determined by group-level random permutation test (54% being the statistical threshold at $P < 0.001$), demonstrating the presence of emotional signals in retinotopic visual areas including V1.

For comparison, whereas univariate analysis identified six ROIs (V3d, hMT, LO1, LO2, V3a, and IPS) as being more activated in pleasant > neutral ($P < 0.05$, FDR corrected), and 11 ROIs (V2v, V3v, V3d, hV4, VO1, VO2, LO1, LO2, hMT, V3a, and IPS) as being more activated in unpleasant > neutral ($P < 0.05$, FDR corrected), multivariate analysis revealed that decoding accuracy in all 17 retinotopic visual ROIs were significantly above chance level for both unpleasant versus neutral decoding and pleasant versus neutral decoding, highlighting the importance of multivoxel-level activity patterns in revealing the full extent of emotional signaling in the retinotopic visual cortex (see Fig. 3C for visualization of retinotopic visual regions revealed by univariate vs. multivariate approaches as containing emotional signals).

Affective pictures are often characterized along two dimensions: valence and arousal. Relative to neutral pictures, pleasant and unpleasant pictures are different both in terms of valence as well as in terms of arousal. We attempted to control for one of the two factors (i.e., normative arousal ratings) by decoding between unpleasant and pleasant pictures. As shown in Figure 4A, there was no significant difference in normative arousal ratings between pleasant and unpleasant pictures ($P = 0.2$, Fig. 4A), but normative valence ratings between them was significantly different ($P < 0.0001$, Fig. 4A). Decoding accuracy between the two classes of pictures in all the retinotopic ROIs was significantly above chance level (Fig. 4B, where 54% is the statistical threshold at $P < 0.001$ according to a random permutation test), suggesting that the differences in multivoxel patterns between pleasant versus neutral and unpleasant versus neutral comparison were not simply driven by emotional intensity of the stimuli.

Reentrant Modulation of Visual Representations of Affective Scenes

It has been well established that viewing emotionally engaging scenes is associated with facilitated visuocortical processing, which can be measured by EEG, fMRI, and behavior. This facilitated processing is thought to be the consequence of reentrant signals that arise from emotion-modulated deep brain structures such as the amygdala and back-project into the visual system, in particular the VVC, to modulate visual processing. This hypothesis would be supported and extended to the domain of multivoxel neural representations if decoding accuracy in retinotopic areas is parametrically related to evidence of feedback signaling. To examine this issue, we divided the retinotopic ROIs into three broader visual regions based on consistency of anatomical location and functional role: (1) early visual cortex (EVC), located on the posterior portion of the occipital lobe and involved in perception of basic visual features (Sereno et al. 1995; DeYoe et al. 1996; Engel et al. 1997), which included v1v, v1d, v2v, v2d, v3v, v3d; (2) dorsal visual cortex (DVC), located along dorsal parietal pathway and known to carry out motor and high-order spatial functions such as motion perception, spatial attention, and motor preparation (Bressler et al. 2008; Konen and Kastner 2008; Wandell and Winawer 2011), which included the combined ROIs of IPS; and (3) VVC, located along ventral temporal pathway and known to be involved in object and scene recognition (Brewer et al. 2005; Arcaro et al. 2009), which included VO1, VO2, PHC1, and PHC2. The visualized anatomical location of the three broader visual regions is shown in Figure 5A. We expected that VVC, anatomically shown as the visual structure that receives major feedback projections from the medial temporal and frontal regions (Amaral et al. 2003; Vuilleumier et al. 2004; Freese and Amaral 2005), would show significant correlation between decoding accuracy and the strength of signal reentry.

First, using LPP as an index of signal reentry, we correlated the decoding accuracy in EVC, VVC, and DVC with LPP. As shown in Figure 5B, for VVC, unpleasant versus neutral decoding accuracy and LPP amplitude were significantly correlated ($R = 0.69$, $P = 0.0008$); pleasant versus neutral decoding accuracy in VVC was also significantly correlated with LPP amplitude, albeit with a smaller R value ($R = 0.50$, $P = 0.026$). LPP was not significantly correlated with unpleasant versus neutral decoding accuracy in either EVC ($R = 0.37$, $P = 0.11$) or DVC ($R = 0.36$, $P = 0.12$). Similarly, LPP was not significantly correlated with pleasant versus neutral decoding accuracy in either EVC ($R = 0.34$, $P = 0.14$) or DVC ($R = 0.29$, $P = 0.22$).

Next, assessing the amygdala to VVC feedback more directly via DAG, a measure of directed connectivity, we computed amygdala→VVC EC and correlated it with the decoding accuracy in VVC. Amygdala→VVC EC and VVC unpleasant versus neutral decoding accuracy was significantly correlated ($r = 0.66$, $P = 0.001$) (Fig. 5D, left), whereas amygdala→VVC EC and VVC pleasant versus neutral decoding accuracy was not significantly correlated ($r = 0.27$, $P = 0.25$) (Fig. 5D, right). We then conducted a whole-brain EC analysis using VVC as the seed. EC from each voxel in the brain to VVC was computed and correlated with VVC decoding accuracy. Voxels with correlation coefficient exceeding 0.61 ($P < 0.005$) and being part of a contiguous cluster of >10 such voxels were considered significant. For pleasant versus neutral comparison, as shown in Figure 6A, the potential sources of reentrant signals are bilateral superior temporal sulcus (STS)/superior temporal gyrus (STG) regions, right IFG, and right ventral lateral prefrontal cortex (VLPFC), whereas for unpleasant versus neutral comparison, the potential sources of reentrant signals are the amygdala, agreeing with the result from the ROI-based analysis, and the right STS/STG region (Fig. 6C). To examine the collective contribution of the reentry from these regions to the neural representations of emotional pictures in VVC, we constructed a multiple regression model using VVC decoding accuracy as the predicted variable and the following ECs as the predictor variables: Pleasant: IFG→VVC, VLPFC→VVC, and STS/STG→VVC; Unpleasant: Amygdala→VVC and STS/STG→VVC. Mathematically, for pleasant, the model can be written as: $\text{VVC decoding accuracy} = \beta_0 + \beta_1 * \text{EC}(\text{IFG} \rightarrow \text{VVC}) + \beta_2 * \text{EC}(\text{VLPFC} \rightarrow \text{VVC}) + \beta_3 * \text{EC}(\text{STS/STG} \rightarrow \text{VVC}) + \epsilon$; for unpleasant, the model can be written as: $\text{VVC decoding accuracy} = \beta_0 + \beta_1 * \text{EC}(\text{Amygdala} \rightarrow \text{VVC}) + \beta_2 * \text{EC}(\text{STS/STG} \rightarrow \text{VVC}) + \epsilon$. Here, EC stands for effective connectivity. As shown in Figure 6B and D, the predicted decoding accuracy is strongly correlated with actual VVC decoding accuracy ($R = 0.95$ for pleasant vs. neutral decoding and $R = 0.84$ for unpleasant vs. neutral decoding, $P < 0.0001$), demonstrating that a large portion of the variance in VVC decoding accuracy can be explained by EC from anterior temporal and prefrontal regions back to VVC.

A further analysis was carried out to test whether LPP as an index of signal reentry is linearly related to the frontotemporal EC to VVC. Again, a multiple regression model was used with LPP as the predicted variable and ECs as the predictor variables. That is, for Pleasant, $\text{LPP} = \beta_0 + \beta_1 * \text{EC}(\text{IFG} \rightarrow \text{VVC}) + \beta_2 * \text{EC}(\text{VLPFC} \rightarrow$

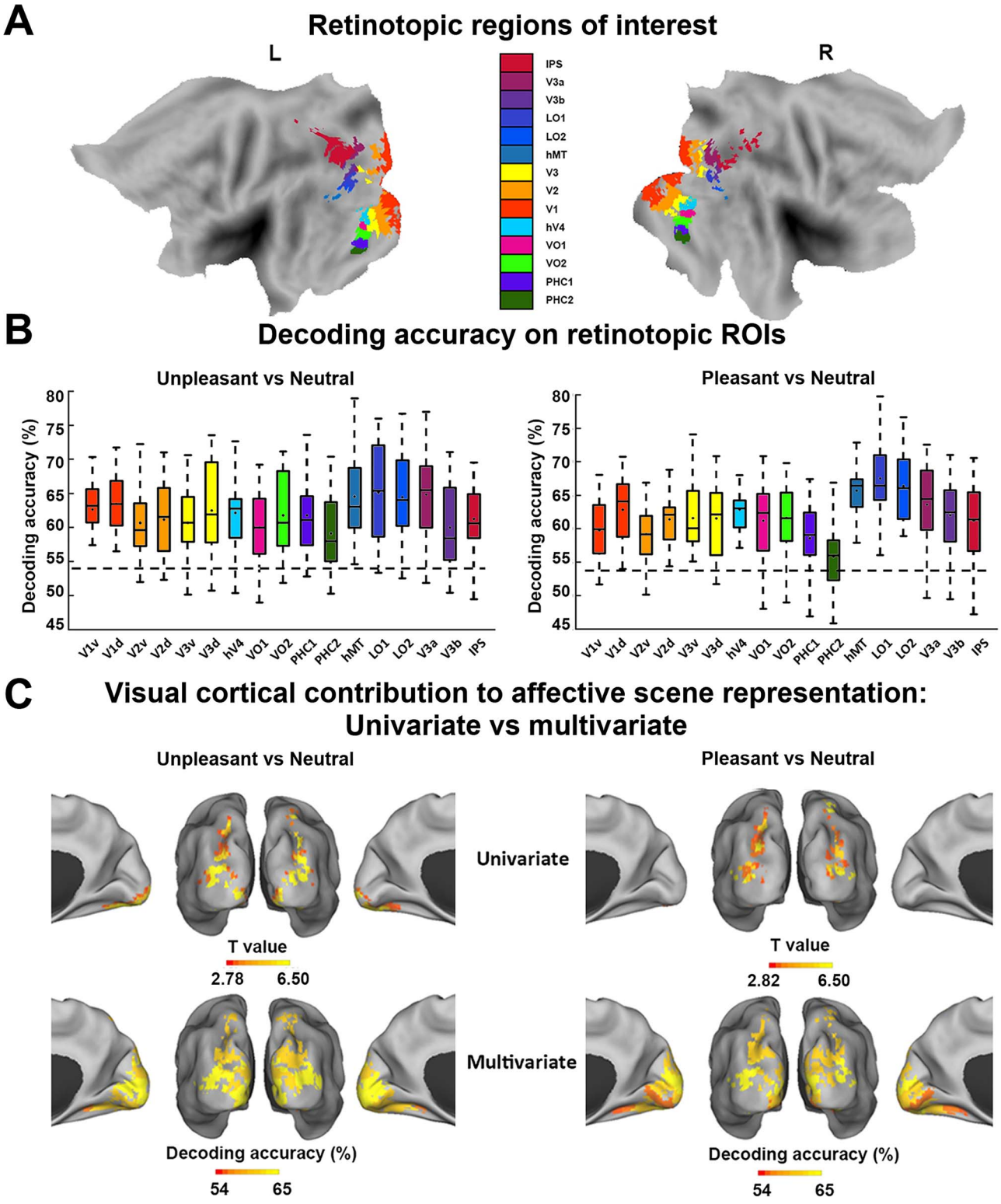

Figure 3. MVPA decoding analysis of neural representations of emotional scenes in retinotopic visual cortex. (*A*) Retinotopic ROIs visualized on the flattened brain. (*B*) Group average decoding accuracy between unpleasant versus neutral and pleasant versus neutral in different ROIs. Dashed line indicates the statistical significance threshold (54%). (*C*) Comparison between visual cortical contribution to the representation of affective scenes revealed by (top) univariate activation analysis (data from Fig. 2A,B replotted here) and by (bottom) multivariate decoding from B.

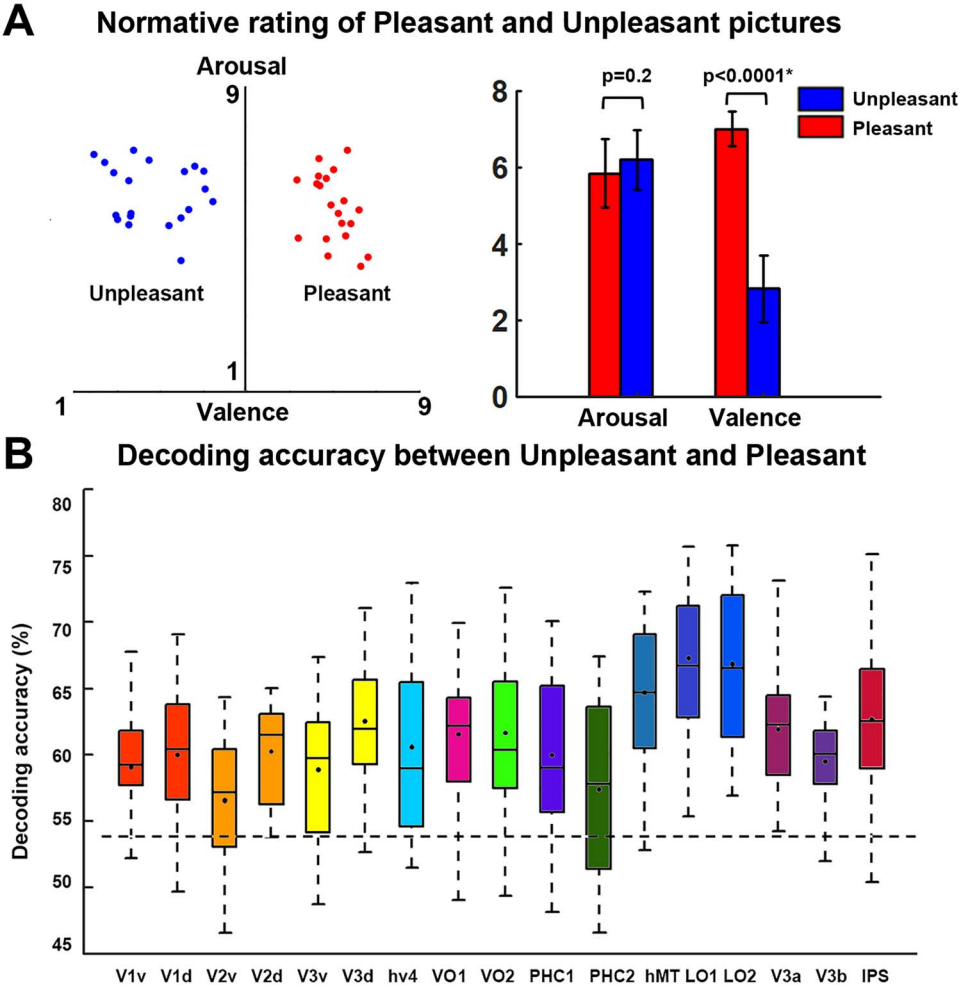

Figure 4. MVPA decoding of pleasant versus unpleasant scenes. (*A*) Normative valence and arousal ratings of unpleasant and pleasant images used in this study. The error bar depicts the standard error of the mean for the normative ratings of 20 pictures in one category. Arousal is not significantly different between the two classes of pictures, whereas pleasant pictures have significantly higher valence than unpleasant pictures. (*B*) Group average decoding accuracy between unpleasant and pleasant in retinotopic ROIs. Dashed line indicates the statistical significance threshold (54%) at $P < 0.001$ according to a random permutation test.

VVC) + β_3 * EC(STS/STG → VVC) + ϵ; and for Unpleasant, LPP = $\beta_0 + \beta_1$ * EC(Amygdala → VVC) + β_2 * EC(STS/STG → VVC) + ϵ. The predicted LPP and the recorded LPP for pleasant pictures and for unpleasant pictures were correlated at $R = 0.63$ ($P = 0.002$) and $R = 0.56$ ($P = 0.01$), respectively. These results provide further support to prior assertions that LPP is an index of signal reentry and shed light on the specific frontotemporal sources of these reentrant signals.

Picture Repetition Effects

In our paradigm, each of the 60 pictures was repeated five times across five runs or sessions (Fig. 1). We tested whether there were repetition effects on LPP amplitude and decoding accuracy across the five runs. As shown in Figure 7A, LPP enhancement across runs exhibited a slightly negative average slope, but the slope was not significantly different from zero (pleasant vs. neutral: $t = -0.67$, $P = 0.51$, $d = 0.15$; unpleasant vs. neutral: $t = -1.44$, $P = 0.17$, $d = 0.32$). Linear fits to LPP enhancement across runs at the individual participant level were shown in Figure 7B. These results, indicating a lack of significant repetition effects on LPP, were consistent with a previous report (Schupp et al. 2006). Decoding accuracy, averaged over all retinotopic regions, was shown as a function of run in Figure 7C. Here, for a given run, an SVM classifier was trained on the data from the other four runs and tested on the data from the given run. The average slope was again slightly negative, but was not significantly different from zero for either pleasant versus neutral decoding ($t = -1.48$, $P = 0.16$, $d = 0.33$) or unpleasant versus neutral decoding ($t = -1.92$, $P = 0.07$, $d = 0.43$). Linear fits to decoding accuracy across runs at the individual participant level were shown in Figure 7D. The negative slopes in Figure 7C, while not statistically different from zero, were nevertheless associated with a small effect size, and may thus still prompt the hypothesis that decoding accuracy declines with repetition over runs.

Discussion

We examined the neural representations of affective scenes by recording simultaneous EEG-fMRI from subjects viewing pleasant, unpleasant, and neutral pictures from the IAPS library. Consistent with previous reports, relative to neutral scenes, both pleasant and unpleasant scenes evoked enhanced LPP on

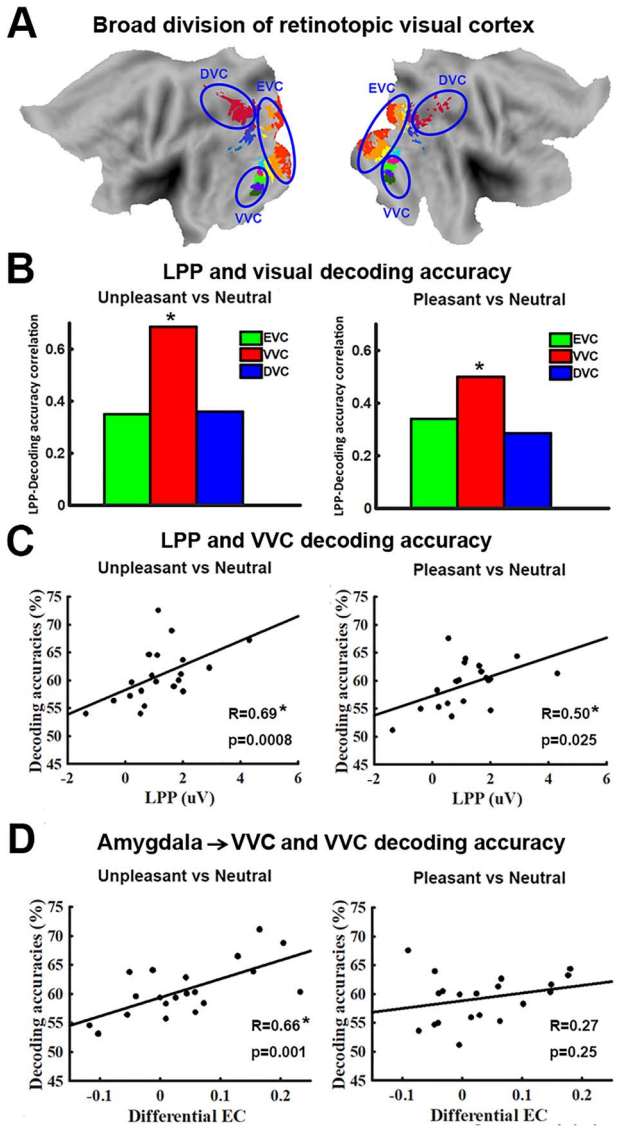

Figure 5. Relation between decoding accuracy and measures of signal reentry. (*A*) Anatomical location of EVC, VVC, and DVC on flattened brain. (*B*) LPP – decoding accuracy correlation for unpleasant versus neutral (left) and pleasant versus neutral (right) in EVC, VVC, and DVC. Only decoding accuracy in VVC is significantly correlated with LPP. (*C*) Scatter plots showing relationship between LPP and decoding accuracy for unpleasant versus neutral (left) and pleasant versus neutral (right) in VVC. (*D*) Relationship between amygdala→VVC effective connectivity (EC) and decoding accuracy in VVC. This relationship is only significant in unpleasant versus neutral decoding (*$P < 0.05$).

the scalp and stronger BOLD activation in a large-scale brain network that included limbic and frontal structures as well as higher-order visual cortices. Applying MVPA to retinotopic visual ROIs, we further found that the multivoxel patterns evoked by pleasant and unpleasant scenes were distinct from one another and from those evoked by neutral scenes in all retinotopic visual regions, including the primary visual cortex V1. Concurrently recorded LPP amplitude, an electrophysiological index of recurrent signaling between anterior brain areas and visual cortex, was shown to predict decoding accuracy in VVC. This was corroborated by an EC analysis using DAG, which demonstrated that for unpleasant scenes, the amygdala was a likely source of the reentrant signals, whereas for the pleasant scenes, frontal lobe structures including right IFG and right VLPFC were found to be the likely sources of the reentrant signals.

Representation of Emotional Scenes in Retinotopic Visual Cortex

The canonical network selectively activated by affective scenes includes anterior temporal lobe, limbic structures, and prefrontal cortex (Sabatinelli et al. 2011). Mixed findings, however, have been reported regarding the involvement of retinotopic visual areas in the representation of emotional content. Many electrophysiological studies have reported differential retinotopic responses to emotional versus neutral visual cues, both in human observers (Keil et al. 2003; Thigpen et al. 2017; Li 2019) as well as in experimental animals (Li et al. 2019). Similarly, the existence of emotion-specific signals in retinotopic areas is predicted by theoretical work based on animal model data (Amaral et al. 2003) as well as on computational models (Kragel et al. 2019). By contrast, univariate BOLD analyses of retinotopic ROIs, including all early visual areas, tend to not show differences in activation as a function of emotional content (Sabatinelli et al. 2009; meta-analysis in Sabatinelli et al. 2011). This well-established finding was also replicated in the present report, where retinotopic visual areas as well as some higher-order visual cortices like PHC1, PHC2, and V3b were found to be not differentially activated by emotional pictures. Only after we applied multivariate techniques did we find strong evidence for emotion-specific visuocortical engagement across a wide range of retinotopic visual regions including primary visual cortex V1.

In univariate fMRI analysis, for a voxel to be reported as activated by an experimental condition, it needs to be consistently activated across individuals. As such, individual differences in voxel activation patterns could lead to failure to detect the presence of neural activity in a given region of the brain. MVPA overcomes this limitation. In MVPA, multivoxel patterns of activation within a ROI are the unit of analysis, and pattern differences between experimental conditions are assessed at the individual subject level, followed by summary statistics computed at the population level (e.g., decoding accuracy averaged across participants). In the past decade, studies have begun to apply MVPA to paradigms where emotional stimuli were used (Said et al. 2010; Sitaram et al. 2011; Baucom et al. 2012; Kotz et al. 2013; Saarimäki et al. 2015; see Kragel and LaBar 2014 for review). Our study extends this line of research. When multivoxel patterns of neural activation between emotion and neutral pictures were compared, all retinotopic visual cortices, including primary visual cortex, were shown to contain affective signals.

Affective pictures are characterized along two dimensions: valence and arousal. When decoding unpleasant versus pleasant viewing conditions, in which emotional arousal ratings were largely matched, it was found that the decoding accuracy was above chance in all the visual ROIs, suggesting that valence-specific information is encoded in retinotopic visual cortex. This result is consistent with previous work showing that affective valence modulates the gating of early visual input and scope of sensory encoding (Schmitz et al. 2009). The observation that valence-specific information is coded in visual areas is also consistent with an emerging theoretical framework (Miskovic and Anderson 2018; Todd et al. 2020), supported by multivariate

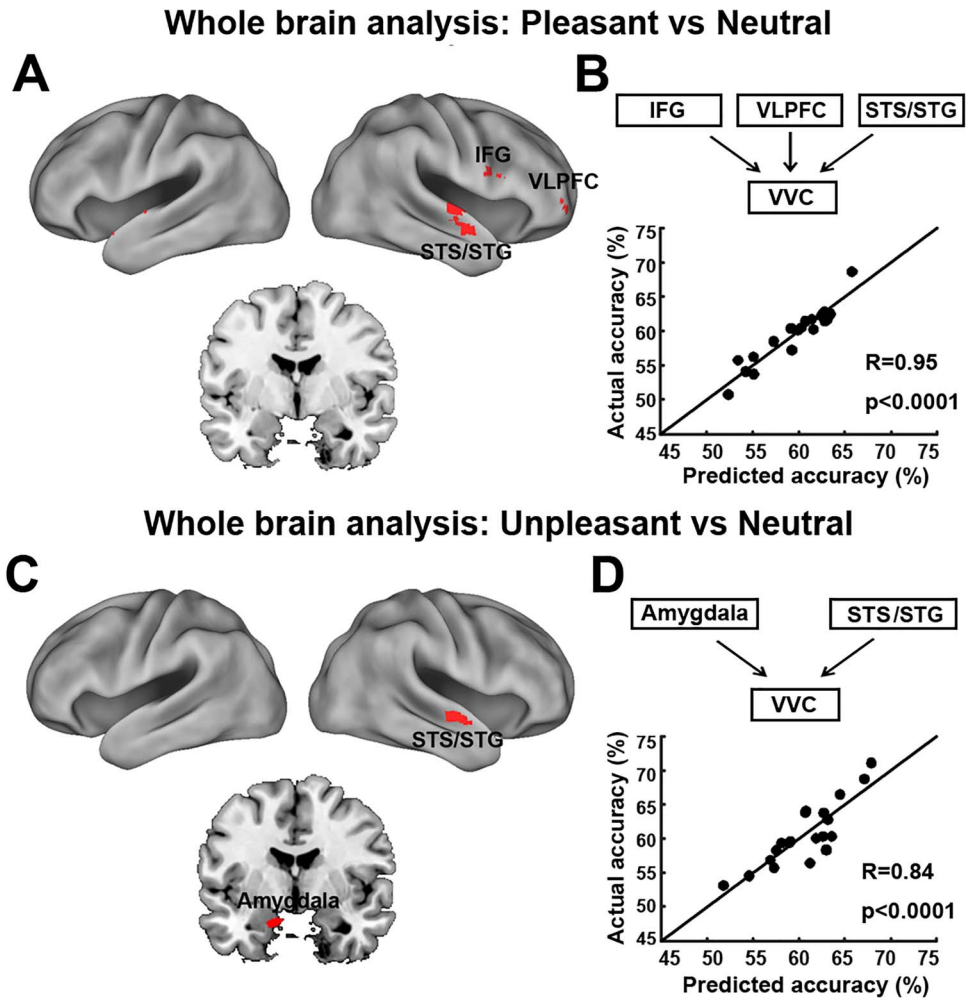

Figure 6. VVC-seeded whole-brain effective connectivity analysis. (*A*) Brain maps showing voxels whose effective connectivity into VVC predicts VVC pleasant vs neutral decoding accuracy. (*B*) Measured VVC pleasant vs neutral decoding accuracy vs predicted VVC pleasant vs neutral decoding accuracy according to a linear model accounting for the collective contributions of reentry signaling from regions identified in panel A (see Results). (*C*) Brain maps showing voxels whose effective connectivity into VVC predicts VVC unpleasant vs neutral decoding accuracy. (*D*) Measured VVC unpleasant vs neutral decoding accuracy vs predicted VVC unpleasant vs neutral decoding accuracy according to a linear model accounting for the collective contributions of reentry signaling from regions identified in panel C (see Results). STG, superior temporal gyrus; STS, superior temporal sulcus; IFG, inferior frontal gyrus; VLPFC, ventral lateral prefrontal cortex. All maps were thresholded at $R > 0.61$, $p < 0.005$ and clusters containing more than 10 contiguous such voxels are shown.

analyses of fMRI data (Chikazoe et al. 2014), in which sensory representations are inherently characterized by the valence (pleasant and unpleasant) of the represented information (Satpute et al. 2015) in modality-specific sensory areas (Shinkareva et al. 2014). The neurophysiological implications of this view continue to produce interesting questions for future research, because sensory processing itself is an inherently parallel, distributed process (Nassi and Callaway 2009). Thus, although stimulus valence may well be represented similarly to other sensory dimensions extracted from the external world, hypotheses regarding how specific neurocomputations encode these physical and affective dimensions remain to be formulated and tested. Using DAGs, the present study offers one avenue for linking connectivity and decoding analyses to test such hypotheses. Despite the promising results, we hasten to point out that the number of stimuli used in the current study is rather small (20 per category), and that in future studies, a wider range of stimuli combined with more objective stimulus ratings are required to further establish valence modulation of sensory processing.

Although the IAPS pictures used in this study were carefully selected to match for content and image composition, an obvious question is whether the differences in multivoxel patterns between different emotional categories are attributable to differences in physical properties that are of a nonemotional nature. To address this concern, we conducted a control analysis by subdividing neutral pictures into pictures with neutral people and pictures with neutral scenes. As shown in Supplementary Figure S1 of the supplementary materials, decoding accuracy between neutral people and neutral scenes was at chance level within all retinotopic visual regions, suggesting that it is the emotional content of the pictures rather than the physical/categorical composition (e.g., people vs. scenes) that determined the observed pattern differences in the retinotopic regions considered in this study.

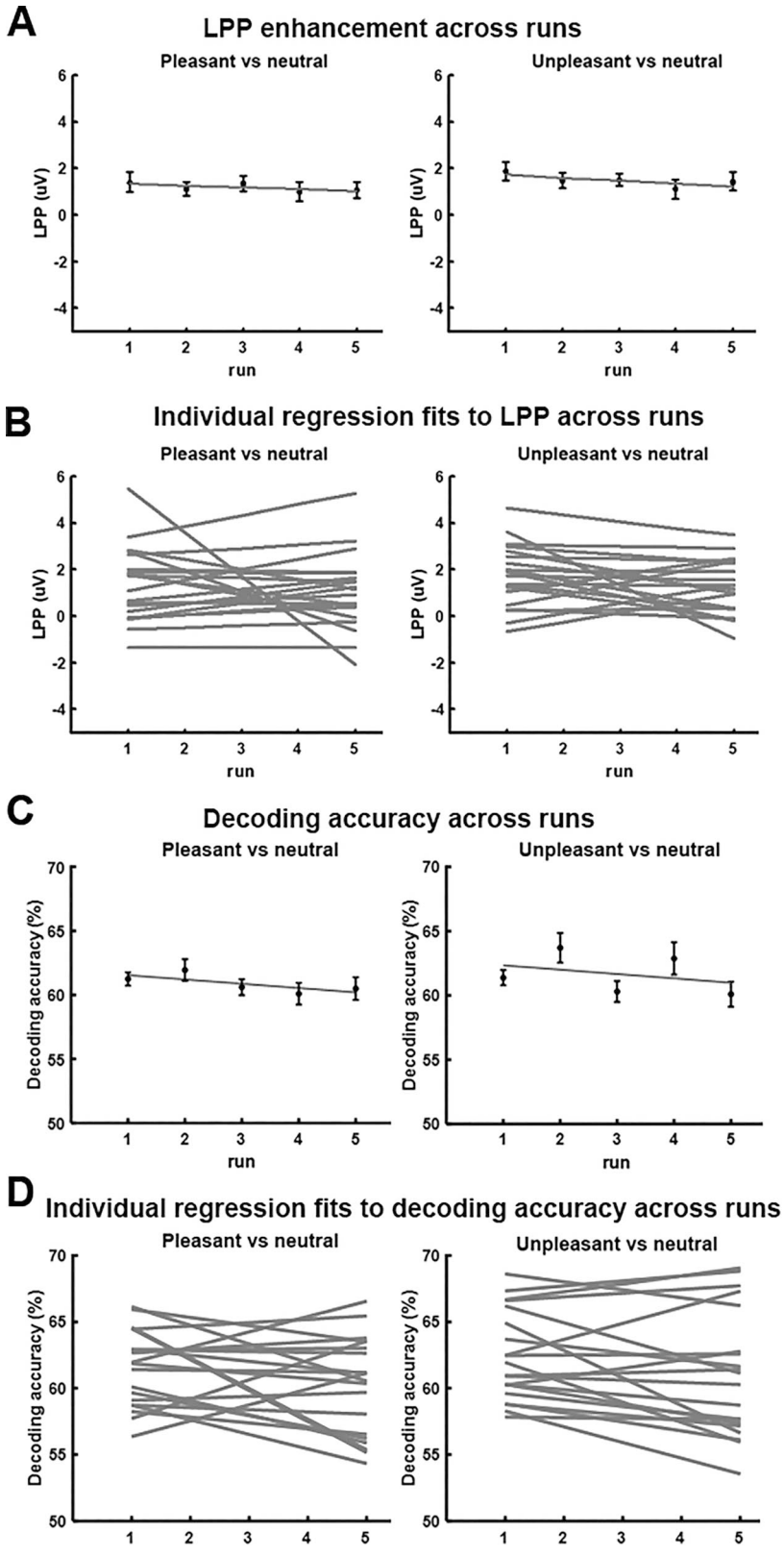

Figure 7. Effects of picture repetition. (*A*) LPP enhancement as a function of run. (*B*) Linear fits to LPP as a function of run for each individual participant ($n = 20$). The slopes were not significantly different from zero ($P = 0.51$ for pleasant vs. neutral and $P = 0.17$ for unpleasant vs. neutral). (*C*) Decoding accuracy as a function of run. (*D*) Linear fits to decoding accuracy as a function of run for each individual participant ($n = 20$). The slopes were not significantly different from zero ($P = 0.16$ for pleasant vs. neutral and $P = 0.07$ for unpleasant vs. neutral).

Among all the visual ROIs considered here, the highest decoding accuracy was consistently observed in LO regions LO1 and LO2. These regions are part of the lateral occipital complex (LOC) and known for their role in object recognition (Larsson and Heeger 2006). A recent fMRI–pupillometry study reports that BOLD activity in LOC is modulated by the valence of the stimulus (Kuniecki et al. 2018). Specifically, by superimposing pink noise on IAPS pictures, these authors found greater increase of LOC activity for unpleasant pictures compared with neutral ones when the noise level is decreased. We subdivided unpleasant scenes into attack scenes and disgust scenes, pleasant scenes into happy people and erotic people, and neutral scenes into neutral people and nature scenes. The pairwise decoding accuracies of the six subcategories, shown in Supplementary Table S3 of the supplementary materials, showed that whereas any two subcategories belonging to two different broad picture categories (e.g., pleasant vs. neutral) are always decodable, the two subcategories within a broad picture category are sometimes decodable (e.g., attack scenes vs. disgust scenes within unpleasant) and sometimes not (e.g., neutral people vs. nature scenes within neutral). These results suggest that the differences in distributed activities in LOC may reflect both semantic differences as well as valence differences. However, as pointed out above, the small number of stimuli used in this study limits our ability to make strong inferences regarding the specific role of LOC in object versus emotion processing.

Role of Reentrant Signals in Visual Representations of Emotion

Where do affective signals in retinotopic visual cortex come from? One recent hypothesis stresses that visual cortex can innately discriminate stimuli varying in affective significance (see Miskovic and Anderson 2018 for a review). For example, both animal model studies and human studies (Weinberger 2004; Thigpen et al. 2017; Li et al. 2019) have found that sensory cortex is able to encode the threat content of a visual stimulus, typically after extensive learning. A recent computational study supported this hypothesis by showing that an artificial deep neural network, whose training requires a large amount of stimuli with repetition, has the ability to encode emotional content (Kragel et al. 2019). In human observers, such differential sensitivity to visual features associated with emotional content may be acquired through daily experience (McTeague et al. 2018). However, given that the exemplars used in the present study were novel for the participants and presented only five times across the duration of the study, it is unlikely that retinotopic visual cortex learned to represent individual features that are linked to emotional significance during the course of the experimental session. Thus, we examined the evidence for the alternative hypothesis that affective signals in retinotopic areas emanate from anterior frontotemporal structures via the mechanism of reentry.

The signal reentry hypothesis proposes that when viewing emotional stimuli, subcortical structures such as the amygdala, upon receiving the initial sensory input, send feedback signals into visual cortex to enhance the processing of the motivationally salient visual input (Keil et al. 2009; Sabatinelli et al. 2009; Lang and Bradley 2010; Pessoa 2010). Such enhanced visual processing prompts increased vigilance towards appetitive or aversive stimuli, ultimately promoting the deployment of adaptive action in the interest of survival. The reentry hypothesis is indirectly supported by neuroanatomy studies showing feedback projections from the amygdala to the ventral visual stream (Amaral et al. 2003; Freese and Amaral 2005). Patients with amygdala lesion tend to show no visual cortex enhancement in response to threat, even when their visual cortex is structurally intact (Vuilleumier et al. 2004). In human imaging studies, it has been shown that BOLD activation in amygdala precedes activation in visual cortex, and the functional connectivity between amygdala and VVC is increased during affective picture viewing (Sabatinelli et al. 2005, 2009). Analysis using Granger causality further demonstrated heightened directional connectivity from amygdala to fusiform cortex when viewing emotional scenes (Sabatinelli et al. 2014; Frank et al. 2019).

To examine how signal reentry is affecting neural representations of affective pictures in retinotopic visual cortex, we first used the LPP to index reentrant processing (Lang et al. 1998; Hajcak et al. 2006; Lang and Bradley 2010), which was well motivated based on prior studies (Liu et al. 2012; Sabatinelli et al. 2013). That the LPP amplitude was statistically significantly correlated with decoding accuracy in VCC, but not in EVC and DVC, is understandable from an anatomical perspective because VVC, beginning at the anterior edge of V4 and extending anteriorly to posterior PHC, receives extensive input from anterior temporal and frontal structures, and is thus expected to be strongly influenced by these structures. Upon receiving reentrant feedback, VVC may also play the role of transmitting the reentrant signals down to EVC. Functionally, given that VVC is involved in object and scene perception, which is essential for the current experimental paradigm requiring participants to perceive static pictures with complex affective contents, the purpose of reentry could be to selectively enhance the visual regions mostly related to the ongoing task.

DVC contains higher-order visual cortex IPS along the dorsal parietal pathway. In our data, decoding accuracy in DVC was higher relative to VVC and EVC, but was not correlated with LPP amplitude, suggesting that neural representations of emotional content in DVC was not influenced by reentry indexed by LPP. Neuroscientifically, DVC is known to play essential roles in visual spatial attention, motion perception, and motor preparation (Bressler et al. 2008; Wandell and Winawer 2011). A previous study using naturalistic emotional videos (Goldberg et al. 2014) reported a preferential activation in the dorsal parietal visual stream, which, the authors hypothesized, was related to motor preparation associated with emotionally salient information. Our results can be seen as lending support to this hypothesis by showing that affective stimuli evoke emotion-specific neural patterns in dorsal association cortices that lie at the interface between visual perception and motor preparation for survival-relevant actions (Lang and Bradley 2010). Furthermore, along with the findings in VVC, our results also suggest that viewing emotional scenes prompts parallel emotional processes along ventral and dorsal visual pathways, serving possibly different functional purposes.

In addition to LPP amplitude, we also used inter-regional EC as an index of reentry, with an initial emphasis on the role of amygdala in generating the feedback signals. The successful indexing for unpleasant emotion lent credence to the idea that the reentrant signals arising from limbic structures modulate the visuocortical representations of negative emotion. Although this relationship is not observed when viewing pleasant pictures, a further whole-brain level EC analysis indicated that for pleasant scenes, the potential sources of reentrant signals include bilateral STS/STG, right IFG, and right VLPFC.

Interpreting this finding, we note that VLPFC has been considered part of the ventral affective system, which includes VLPFC, MPFC, and amygdala (Dolcos and McCarthy 2006). Anatomically, VLPFC has strong connections with sensory areas as well as emotion-modulated structures such as the amygdala and orbitofrontal cortex (Carmichael and Price 1995a, 1995b; Petrides and Pandya 2002; Kennerley and Wallis 2009). The VLPFC integrates reward information and provides top-down signals to sensory cortex to improve behavioral performance (Kennerley and Wallis 2009). Right IFG is known to be involved both in cognitive control tasks and in emotional processing by exerting top-down control of STS/STG (Frye et al. 2010) and ventral sensory stream (Tops and Boksem 2011).

For unpleasant scenes, the whole-brain EC analysis again revealed that the amygdala was an important source of reentrant feedback, along with STS/STG. Whereas the appearance of amygdala in the whole-brain map agrees with and confirms the ROI-based analysis, the appearance of the STS/STG region in the brain map was a new finding; the same STS/STG region appeared both in the processing of pleasant and unpleasant scenes (Narumoto et al. 2001), suggesting that the STS/STG region may serve as a way station, which transmits the signals received from the limbic and/or prefrontal structures to visual cortex. Primate studies have found that STS/STG reciprocally interacts with the ventral visual stream (Cusick 1997; Allison et al. 2000). In addition, STS/STG is structurally connected with the amygdala from which it receives feedback projections (Grezes et al. 2014; Pitcher et al. 2017). Thus, the present study helps advance an interesting hypothesis for further studies to test, which, by integrating animal model work, computational modeling, and advanced neuroimaging in humans, can potentially lead to more precisely defined pathways of neural feedback signaling in emotional scene perception.

In this work, both LPP and EC were used to index signal reentry from frontotemporal cortices. That a large portion of LPP variance was ECs from anterior structures such as amygdala and VLPFC demonstrates that the two measures of signal reentry are related, providing a connectivity-level neural substrate of LPP, which in the previous studies has been mainly linked to activations of distributed brain regions without regards to how these regions functionally interact (Liu et al. 2012; Sabatinelli et al. 2013).

Potential Effects of Picture Repetition

The repetition effects in emotion scene perception are usually studied by presenting the same affective picture in consecutive trials or repeatedly within the same block of trials (Ferrari et al. 2011; Bradley et al. 2015). These studies have consistently found reduced but still robust emotional responses evoked by repeated picture presentations. The effects of picture repetition across blocks, as is the case here, have been shown to be small. For example, Schupp et al. (2006) showed the same 40 IAPS images over 90 runs with the order of presentation varying in each run and found that emotional enhancement measured by ERPs did not vary across runs. We replicated the Schupp et al. (2006) findings by showing that the LPP amplitude did not systematically change across subsequent runs. The effects of picture repetition on fMRI decoding accuracy have not been studied before. Across five runs, the decoding accuracy as a function of run exhibited a negative slope. Although the negative slope is not significantly different from zero, it nevertheless prompts the need to further examine the possible hypothesis in future studies, employing larger number of runs and subjects, which decoding accuracy between different categories of affective scenes could decrease over runs.

Summary and Outlook

We recorded simultaneous EEG-fMRI from participant viewing natural images containing affective scenes. Applying MVPA to fMRI data, we found the presence of affective signals in the entire retinotopic visual cortex, including V1. Using scalp potential LPP as indices of recurrent signaling between anterior brain regions and visual cortex, emotion-sensitive neural representations in the ventral portion of retinotopic visual cortex were found to be related to signal reentry from anterior brain structures. Further analysis using EC identified the sources of these reentrant signals, which include amygdala and STS/STG in the case of unpleasant scene processing and IFG, VLPFC, and STS/STG in the case of pleasant scene processing.

The present analyses focused on the nature and origin of fMRI voxel pattern signatures during emotional picture viewing. Analysis of EEG data was limited to the estimation of LPP, which was used to index recurrent processing among visual and extravisual regions. Future work focusing on the EEG data in greater detail may address questions concerning the temporal dynamics of affective scene processing. In this vein, a recent EEG study (Greene and Hansen 2020) suggests that the perception of naturalistic scenes can be decomposed into multiple stages, where processing of low-level visual features is associated with early visual ERPs, whereas the processing of high-level visual features is associated with late visual ERPs. To what extent similar temporal profiles apply to affective scene perception is unknown. Leveraging the temporal resolution of EEG and spatial resolution of fMRI, the current data is expected to shed light on this question.

Supplementary Material

Supplementary material can be found at *Cerebral Cortex* online.

Notes

Conflict of Interest: None declared.

Funding

National Institutes of Health (grant R01 MH112558).

References

Allen PJ, Josephs O, Turner R. 2000. A method for removing imaging artifact from continuous EEG recorded during functional MRI. *Neuroimage*. 12(2):230–239.

Allen PJ, Polizzi G, Krakow K, Fish DR, Lemieux L. 1998. Identification of EEG events in the MR scanner: the problem of pulse artifact and a method for its subtraction. *Neuroimage*. 8(3):229–239.

Allison T, Puce A, McCarthy G. 2000. Social perception from visual cues: role of the STS region. *Trends Cogn Sci*. 4(7): 267–278.

Amaral DG, Behniea H, Kelly JL. 2003. Topographic organization of projections from the amygdala to the visual cortex in the macaque monkey. *Neuroscience*. 118(4):1099–1120.

Arcaro MJ, McMains SA, Singer BD, Kastner S. 2009. Retinotopic organization of human ventral visual cortex. *J Neurosci*. 29(34):10638–10652.

Baucom LB, Wedell DH, Wang J, Blitzer DN, Shinkareva SV. 2012. Decoding the neural representation of affective states. *Neuroimage*. 59(1):718–727.

Belouchrani A, Abed-Meraim K, Cardoso JF, Moulines E. 1993. Second-order blind separation of temporally correlated sources. In: *Proc Int Conf on Digital Sig Proc*, Cyprus. p. 346–351.

Bradley MM. 2009. Natural selective attention: orienting and emotion. *Psychophysiology*. 46(1):1–11.

Bradley MM, Codispoti M, Cuthbert BN, Lang PJ. 2001. Emotion and motivation I: defensive and appetitive reactions in picture processing. *Emotion*. 1(3):276.

Bradley MM, Costa VD, Ferrari V, Codispoti M, Fitzsimmons JR, Lang PJ. 2015. Imaging distributed and massed repetitions of natural scenes: spontaneous retrieval and maintenance. *Hum Brain Mapp*. 36(4):1381–1392.

Bradley MM, Keil A, Lang PJ. 2012. Orienting and emotional perception: facilitation, attenuation, and interference. *Front Psychol*. 3:493.

Bradley MM, Lang PJ. 1994. Measuring emotion: the self-assessment manikin and the semantic differential. *J Behav Ther Exp Psychiatry*. 25(1):49–59.

Bradley MM, Sabatinelli D, Lang PJ, Fitzsimmons JR, King W, Desai P. 2003. Activation of the visual cortex in motivated attention. *Behav Neurosci*. 117(2):369.

Bressler SL, Tang W, Sylvester CM, Shulman GL, Corbetta M. 2008. Top-down control of human visual cortex by frontal and parietal cortex in anticipatory visual spatial attention. *J Neurosci*. 28(40):10056–10061.

Brewer AA, Liu J, Wade AR, Wandell BA. 2005. Visual field maps and stimulus selectivity in human ventral occipital cortex. *Nat Neurosci*. 8(8):1102–1109.

Bush KA, Inman CS, Hamann S, Kilts CD, James GA. 2017. Distributed neural processing predictors of multi-dimensional properties of affect. *Front Hum Neurosci*. 11:459.

Cacioppo JT, Crites SL, Gardner WL, Berntson GG. 1994. Bioelectrical echoes from evaluative categorizations: I. A late positive brain potential that varies as a function of trait negativity and extremity. *J Pers Soc Psychol*. 67(1): 115.

Carmichael ST, Price JL. 1995a. Limbic connections of the orbital and medial prefrontal cortex in macaque monkeys. *J Comp Neurol*. 363:615–641.

Carmichael ST, Price JL. 1995b. Sensory and premotor connections of the orbital and medial prefrontal cortex of macaque monkeys. *J Comp Neurol*. 363:642–664.

Chang CC, Lin CJ. 2011. LIBSVM: a library for support vector machines. *ACM Trans Intell Syst Technol*. 2(3):27.

Chikazoe J, Lee DH, Kriegeskorte N, Anderson AK. 2014. Population coding of affect across stimuli, modalities and individuals. *Nat Neurosci*. 17(8):1114–1122.

Cusick CG. 1997. The superior temporal polysensory region in monkeys. In: Rockland K, Kaas JH, Peters A, editors, *Cerebral Cortex*, vol. 12. New York: Plenum Press, pp. 435–468.

Cuthbert BN, Schupp HT, Bradley MM, Birbaumer N, Lang PJ. 2000. Brain potentials in affective picture processing: covariation with autonomic arousal and affective report. *Biol Psychol*. 52(2):95–111.

Delorme A, Makeig S. 2004. EEGLAB: an open source toolbox for analysis of single-trial EEG dynamics including independent component analysis. *J Neurosci Methods*. 134(1):9–21.

DeYoe EA, Carman GJ, Bandettini P, Glickman S, Wieser JO, Cox R, Miller D, Neitz J. 1996. Mapping striate and extrastriate visual areas in human cerebral cortex. *Proc Natl Acad Sci*. 93(6):2382–2386.

Dolcos F, McCarthy G. 2006. Brain systems mediating cognitive interference by emotional distraction. *J Neurosci*. 26(7):2072–2079.

Engel SA, Glover GH, Wandell BA. 1997. Retinotopic organization in human visual cortex and the spatial precision of functional MRI. *Cereb Cortex*. 7(2):181–192.

Ethofer T, Van De Ville D, Scherer K, Vuilleumier P. 2009. Decoding of emotional information in voice-sensitive cortices. *Curr Biol*. 19(12):1028–1033.

Ferrari V, Bradley MM, Codispoti M, Lang PJ. 2011. Repetitive exposure: brain and reflex measures of emotion and attention. *Psychophysiology*. 48(4):515–522.

Frank DW, Costa VD, Averbeck BB, Sabatinelli D. 2019. Directional interconnectivity of the human amygdala, fusiform gyrus, and orbitofrontal cortex in emotional scene perception. *J Neurophysiol*. 122(4):1530–1537.

Frank DW, Sabatinelli D. 2017. Primate visual perception: motivated attention in naturalistic scenes. *Front Psychol*. 8:226.

Freese JL, Amaral DG. 2005. The organization of projections from the amygdala to visual cortical areas TE and V1 in the macaque monkey. *J Comp Neurol*. 486(4):295–317.

Frye RE, Wu M-H, Liederman J, McGraw Fisher J. 2010. Greater pre-stimulus effective connectivity from the left inferior frontal area to other areas is associated with better phonological decoding in dyslexic readers. *Front Syst Neurosci*. 4:156.

Goldberg H, Preminger S, Malach R. 2014. The emotion–action link? Naturalistic emotional stimuli preferentially activate the human dorsal visual stream. *Neuroimage*. 84:254–264.

Greene MR, Hansen BC. 2020. Disentangling the independent contributions of visual and conceptual features to the spatiotemporal dynamics of scene categorization. *J Neurosci*. 40(27):5283–5299.

Grezes J, Valabregue R, Gholipour B, Chevallier C. 2014. A direct amygdala-motor pathway for emotional displays to influence action: a diffusion tensor imaging study. *Hum Brain Mapp*. 35(12):5974–5983.

Hajcak G, Moser JS, Simons RF. 2006. Attending to affect: appraisal strategies modulate the electrocortical response to arousing pictures. *Emotion*. 6(3):517.

Hamann S, Herman RA, Nolan CL, Wallen K. 2004. Men and women differ in amygdala response to visual sexual stimuli. *Nat Neurosci*. 7(4):411–416.

Kang D, Liu Y, Miskovic V, Keil A, Ding M. 2016. Large scale functional brain connectivity during emotional engagement as revealed by beta-series correlation analysis. *Psychophysiology*. 53(11):1627–1638.

Keil A, Bradley MM, Hauk O, Rockstroh B, Elbert T, Lang PJ. 2002. Large-scale neural correlates of affective picture processing. *Psychophysiology*. 39(5):641–649.

Keil A, Gruber T, Müller MM, Moratti S, Stolarova M, Bradley MM, Lang PJ. 2003. Early modulation of visual perception by emotional arousal: evidence from steady-state visual evoked brain potentials. *Cogn Affect Behav Neurosci*. 3(3):195–206.

Keil A, Müller MM, Gruber T, Wienbruch C, Stolarova M, Elbert T. 2001. Effects of emotional arousal in the cerebral hemispheres: a study of oscillatory brain activity and event-related potentials. *Clin Neurophysiol*. 112(11):2057–2068.

Keil A, Sabatinelli D, Ding M, Lang PJ, Ihssen N, Heim S. 2009. Re-entrant projections modulate visual cortex in affective

perception: evidence from Granger causality analysis. *Hum Brain Mapp*. 30(2):532–540.
Kennerley SW, Wallis JD. 2009. Reward-dependent modulation of working memory in lateral prefrontal cortex. *J Neurosci*. 29(10):3259–3270.
Kragel PA, LaBar KS. 2014. Advancing emotion theory with multivariate pattern classification. *Emotion Review*. 6(2):160–174.
Kragel PA, Reddan MC, LaBar KS, Wager TD. 2019. Emotion schemas are embedded in the human visual system. *Sci Adv*. 5(7):eaaw4358.
Konen CS, Kastner S. 2008. Representation of eye movements and stimulus motion in topographically organized areas of human posterior parietal cortex. *J Neurosci*. 28(33):8361–8375.
Kotz SA, Kalberlah C, Bahlmann J, Friederici AD, Haynes JD. 2013. Predicting vocal emotion expressions from the human brain. *Hum Brain Mapp*. 34(8):1971–1981.
Kuniecki M, Wołoszyn K, Domagalik A, Pilarczyk J. 2018. Disentangling brain activity related to the processing of emotional visual information and emotional arousal. *Brain Struct Funct*. 223(4):1589–1597.
Lane RD, Reiman EM, Bradley MM, Lang PJ, Ahern GL, Davidson RJ, Schwartz GE. 1997. Neuroanatomical correlates of pleasant and unpleasant emotion. *Neuropsychologia*. 35(11):1437–1444.
Lang PJ, Bradley MM. 2010. Emotion and the motivational brain. *Biol Psychol*. 84(3):437–450.
Lang PJ, Bradley MM, Cuthbert BN. 1997. *International Affective Picture System (IAPS): technical manual and affective ratings*. Gainesville, Florida, USA: NIMH Center for the Study of Emotion and Attention, pp. 39–58.
Lang PJ, Bradley MM, Fitzsimmons JR, Cuthbert BN, Scott JD, Moulder B, Nangia V. 1998. Emotional arousal and activation of the visual cortex: an fMRI analysis. *Psychophysiology*. 35(2):199–210.
Lang PJ, Greenwald MK, Bradley MM, Hamm AO. 1993. Looking at pictures: affective, facial, visceral, and behavioral reactions. *Psychophysiology*. 30(3):261–273.
Larsson J, Heeger DJ. 2006. Two retinotopic visual areas in human lateral occipital cortex. *J Neurosci*. 26(51):13128–13142.
Li W. 2019. Perceptual mechanisms of anxiety and its disorders. In: Olatunji BO, editor. *The Cambridge handbook of anxiety and related disorders*. Cambridge, United Kingdom: Cambridge University Press, pp. 59–88.
Li Z, Yan A, Guo K, Li W. 2019. Fear-related signals in the primary visual cortex. *Curr Biol*. 29(23):4078–4083.
Liu Y, Huang H, McGinnis-Deweese M, Keil A, Ding M. 2012. Neural substrate of the late positive potential in emotional processing. *J Neurosci*. 32(42):14563–14572.
Liu Y, Wu X, Zhang J, Guo X, Long Z, Yao L. 2015. Altered effective connectivity model in the default mode network between bipolar and unipolar depression based on resting-state fMRI. *J Affect Disord*. 182:8–17.
Marrelec G, Kim J, Doyon J, Horwitz B. 2009. Large-scale neural model validation of partial correlation analysis for effective connectivity investigation in functional MRI. *Hum Brain Mapp*. 30(3):941–950.
McTeague LM, Gruss LF, Keil A. 2015. Aversive learning shapes neuronal orientation tuning in human visual cortex. *Nat Commun*. 6:7823.
McTeague LM, Laplante M-C, Bulls HW, Shumen JR, Lang PJ, Keil A. 2018. Face perception in social anxiety: visuocortical dynamics reveal propensities for hypervigilance or avoidance. *Biol Psychiatry*. 83(7):618–628.
Miskovic V, Anderson A. 2018. Modality general and modality specific coding of hedonic valence. *Curr Opin Behav Sci*. 19:91–97.
Miskovic V, Keil A. 2012. Acquired fears reflected in cortical sensory processing: a review of electrophysiological studies of human classical conditioning. *Psychophysiology*. 49(9):1230–1241.
Mumford JA, Turner BO, Ashby FG, Poldrack RA. 2012. Deconvolving BOLD activation in event-related designs for multivoxel pattern classification analyses. *Neuroimage*. 59(3):2636–2643.
Narumoto J, Okada T, Sadato N, Fukui K, Yonekura Y. 2001. Attention to emotion modulates fMRI activity in human right superior temporal sulcus. *Cogn Brain Res*. 12(2):225–231.
Nassi JJ, Callaway EM. 2009. Parallel processing strategies of the primate visual system. *Nat Rev Neurosci*. 10(5):360–372.
Norman KA, Polyn SM, Detre GJ, Haxby JV. 2006. Beyond mind-reading: multi-voxel pattern analysis of fMRI data. *Trends Cogn Sci*. 10(9):424–430.
Norris CJ, Chen EE, Zhu DC, Small SL, Cacioppo JT. 2004. The interaction of social and emotional processes in the brain. *J Cogn Neurosci*. 16:1818–1829.
Pastor MC, Bradley MM, Löw A, Versace F, Moltó J, Lang PJ. 2008. Affective picture perception: emotion, context, and the late positive potential. *Brain Res*. 1189:145–151.
Peelen MV, Atkinson AP, Vuilleumier P. 2010. Supramodal representations of perceived emotions in the human brain. *J Neurosci*. 30(30):10127–10134.
Pessoa L. 2010. Emotion and cognition and the amygdala: from "what is it?" to "what's to be done?". *Neuropsychologia*. 48(12):3416–3429.
Pessoa L, McKenna M, Gutierrez E, Ungerleider LG. 2002. Neural processing of emotional faces requires attention. *Proc Natl Acad Sci*. 99(17):11458–11463.
Petrides M, Pandya DN. 2002. Comparative cytoarchitectonic analysis of the human and the macaque ventrolateral prefrontal cortex and corticocortical connection patterns in the monkey. *Eur J Neurosci*. 16:291–310.
Phan KL, Wager T, Taylor SF, Liberzon I. 2002. Functional neuroanatomy of emotion: a meta-analysis of emotion activation studies in PET and fMRI. *Neuroimage*. 16(2):331–348.
Phelps EA, Ling S, Carrasco M. 2006. Emotion facilitates perception and potentiates the perceptual benefits of attention. *Psychol Sci*. 17(4):292–299.
Pitcher D, Japee S, Rauth L, Ungerleider LG. 2017. The superior temporal sulcus is causally connected to the amygdala: a combined TBS-fMRI study. *J Neurosci*. 37(5):1156–1161.
Saarimäki H, Gotsopoulos A, Jääskeläinen IP, Lampinen J, Vuilleumier P, Hari R, Sams M, Nummenmaa L. 2015. Discrete neural signatures of basic emotions. *Cereb Cortex*. 26(6):2563–2573.
Sabatinelli D, Bradley MM, Fitzsimmons JR, Lang PJ. 2005. Parallel amygdala and inferotemporal activation reflect emotional intensity and fear relevance. *Neuroimage*. 24(4):1265–1270.
Sabatinelli D, Fortune EE, Li Q, Siddiqui A, Krafft C, Oliver WT, Beck S, Jeffries J. 2011. Emotional perception: meta-analyses of face and natural scene processing. *Neuroimage*. 54(3):2524–2533.
Sabatinelli D, Frank DW, Wanger TJ, Dhamala M, Adhikari BM, Li X. 2014. The timing and directional connectivity of human frontoparietal and ventral visual attention networks in emotional scene perception. *Neuroscience*. 277:229–238.
Sabatinelli D, Keil A, Frank DW, Lang PJ. 2013. Emotional perception: correspondence of early and late event-related

potentials with cortical and subcortical functional MRI. *Biol Psychol*. 92(3):513–519.

Sabatinelli D, Lang PJ, Bradley MM, Costa VD, Keil A. 2009. The timing of emotional discrimination in human amygdala and ventral visual cortex. *J Neurosci*. 29(47):14864–14868.

Said CP, Moore CD, Engell AD, Todorov A, Haxby JV. 2010. Distributed representations of dynamic facial expressions in the superior temporal sulcus. *J Vis*. 10(5):11.

Sato W, Kochiyama T, Yoshikawa S, Naito E, Matsumura M. 2004. Enhanced neural activity in response to dynamic facial expressions of emotion: an fMRI study. *Cogn Brain Res*. 20(1):81–91.

Satpute AB, Kang J, Bickart KC, Yardley H, Wager TD, Barrett LF. 2015. Involvement of sensory regions in affective experience: a meta-analysis. *Front Psychol*. 6:1860.

Schlösser R, Gesierich T, Kaufmann B, Vucurevic G, Hunsche S, Gawehn J, Stoeter P. 2003. Altered effective connectivity during working memory performance in schizophrenia: a study with fMRI and structural equation modeling. *Neuroimage*. 19(3):751–763.

Schmitz TW, De Rosa E, Anderson AK. 2009. Opposing influences of affective state valence on visual cortical encoding. *J Neurosci*. 29(22):7199–7207.

Schupp HT, Cuthbert BN, Bradley MM, Cacioppo JT, Ito T, Lang PJ. 2000. Affective picture processing: the late positive potential is modulated by motivational relevance. *Psychophysiology*. 37(2):257–261.

Schupp HT, Markus J, Weike AI, Hamm AO. 2003. Emotional facilitation of sensory processing in the visual cortex. *Psychol Sci*. 14(1):7–13.

Schupp HT, Stockburger J, Codispoti M, Junghöfer M, Weike AI, Hamm AO. 2006. Stimulus novelty and emotion perception: the near absence of habituation in the visual cortex. *Neuroreport*. 17(4):365–369.

Sereno MI, Dale AM, Reppas JB, Kwong KK, Belliveau JW, Brady TJ, Rosen BR, Tootell RB. 1995. Borders of multiple visual areas in humans revealed by functional magnetic resonance imaging. *Science*. 268(5212):889–893.

Shimizu S, Hoyer PO, Hyvarinen A, Kerminen A. 2006. A linear non-Gaussian acyclic model for causal discovery. *J Mach Learn Res*. 7:2003–2030.

Shimizu S, Inazumi T, Sogawa Y, Hyvärinen A, Kawahara Y, Washio T, Hoyer PO, Bollen K. 2011. DirectLiNGAM: a direct method for learning a linear non-Gaussian structural equation model. *J Mach Learn Res*. 12:1225–1248.

Shinkareva SV, Wang J, Kim J, Facciani MJ, Baucom LB, Wedell DH. 2014. Representations of modality-specific affective processing for visual and auditory stimuli derived from functional magnetic resonance imaging data. *Hum Brain Mapp*. 35(7):3558–3568.

Sitaram R, Lee S, Ruiz S, Rana M, Veit R, Birbaumer N. 2011. Real-time support vector classification and feedback of multiple emotional brain states. *Neuroimage*. 56(2):753–765.

Stelzer J, Chen Y, Turner R. 2013. Statistical inference and multiple testing correction in classification-based multi-voxel pattern analysis (MVPA): random permutations and cluster size control. *Neuroimage*. 65:69–82.

Thigpen NN, Bartsch F, Keil A. 2017. The malleability of emotional perception: short-term plasticity in retinotopic neurons accompanies the formation of perceptual biases to threat. *J Exp Psychol Gen*. 146(4):464–471.

Todd RM, Miskovic V, Chikazoe J, Anderson AK. 2020. Emotional objectivity: neural representations of emotions and their interaction with cognition. *Annu Rev Psychol*. 71(1): 25–48.

Tops M, Boksem MA. 2011. A potential role of the inferior frontal gyrus and anterior insula in cognitive control, brain rhythms, and event-related potentials. *Front Psychol*. 2: 330.

Vuilleumier P. 2005. How brains beware: neural mechanisms of emotional attention. *Trends Cogn Sci*. 9(12):585–594.

Vuilleumier P, Richardson MP, Armony JL, Driver J, Dolan RJ. 2004. Distant influences of amygdala lesion on visual cortical activation during emotional face processing. *Nat Neurosci*. 7(11):1271.

Wandell BA, Winawer J. 2011. Imaging retinotopic maps in the human brain. *Vision Res*. 51(7):718–737.

Wang L, Mruczek RE, Arcaro MJ, Kastner S. 2015. Probabilistic maps of visual topography in human cortex. *Cereb Cortex*. 25(10):3911–3931.

Weinberger NM. 2004. Specific long-term memory traces in primary auditory cortex. *Nat Rev Neurosci*. 5(4):279–290.